Left-right loading dependence of shock response of (111)//(112) Cu bicrystals: Deformation and spallation

Q. An, W. Z. Han, S. N. Luo, T. C. Germann, D. L. Tonks et al.

Related Articles

Additional information on J. Appl. Phys.

Left-right loading dependence of shock response of (111)//(112) Cu bicrystals: Deformation and spallation

Q. An,[1] W. Z. Han,[2] S. N. Luo,[2,a)] T. C. Germann,[2] D. L. Tonks,[2] and W. A. Goddard III[1]
[1]*Materials and Process Simulation Center, California Institute of Technology, Pasadena, California 91125, USA*
[2]*Los Alamos National Laboratory, Los Alamos, New Mexico 87545, USA*

We investigate with molecular dynamics the dynamic response of Cu bicrystals with a special asymmetric grain boundary (GB), (111)//(112)⟨110⟩, and its dependence on the loading directions. Shock loading is applied along the GB normal either from the left or right to the GB. Due to the structure asymmetry, the bicrystals demonstrate overall strong left-right loading dependence of its shock response, including compression wave features, compression and tensile plasticity, damage characteristics (e.g., spall strength), effective wave speeds and structure changes, except that spallation remains dominated by the GB damage regardless of the loading directions. The presence or absence of transient microtwinning also depends on the loading directions. © *2012 American Institute of Physics*. [http://dx.doi.org/10.1063/1.3692079]

I. INTRODUCTION

It is almost axiomatic that microstructure (defects and interfaces) plays a critical role in materials deformation and damage. The effects of defects and interfaces on dynamic shock response (plasticity and spallation), in particular grain boundaries (GBs), have been a subject of experimental, theoretical, and simulation efforts.[1–15] Given their relative simplicity, bicrystals allow us to gain certain specific insights without being overwhelmed by the complexities of abundant random GBs, and can serve as model systems or building blocks for studying GB effect on shock response. Molecular dynamics (MD) simulations are advantageous in revealing real-time atomistic scale phenomena and mechanisms not accessible by current experimental techniques.[5–8,10,12,14–17] Previous MD simulations of shock loading of bicrystals examined symmetric or asymmetric coincidence-lattice-site (CSL) GBs in face-centered cubic systems, including Σ5 and Σ11 GBs in Pd, Al, and Cu,[7,8,15] and Σ3 Cu bicrystal nanolayers.[14] In shock loading (as opposed to quasistatic loading), the directionality of wave propagation likely gives rises to the loading-direction dependence of shock response in the presence of structural asymmetry as manifested by an asymmetric GB; for example, the shock may impinge on a GB either from its left or right, but such left-right loading dependence (LRLD) was not investigated previously. Here we study with MD simulations a special, non-CSL asymmetric GB, (111)//(112)⟨110⟩ [Fig. 1(a)]. This GB involves different GB normals (⟨111⟩ and ⟨112⟩) and thus different crystallographic directions for wave propagation across the GB, and the {111} slip planes oriented differently in the constituent single crystals, raising the possibility that plastic deformation and damage show LRLD. Indeed, our results demonstrate pronounced LRLD overall, a combined effect of the microstructure and wave propagation. We present the methodology of MD simulations in Sec. II, and the results and discussion in Sec. III, followed by the conclusion in Sec. IV.

II. METHODOLOGY

Our MD simulations use an accurate embedded-atom-method potential for Cu (Ref. 18) with the LAMMPS (large-scale atomic/molecular massively parallel simulator) package.[19] The (111)//(11$\bar{2}$)[$\bar{1}$10] GBs were synthesized recently,[20] and are peculiar in that the CSL method for constructing GBs is not applicable. We thus create separately two grains, grain I with (111) GB plane and grain II with (11$\bar{2}$) GB plane, and then combine them to form a bicrystal. The x-, y-, and z- axes are along [111], [11$\bar{2}$], and [$\bar{1}$10] in grain I and along [11$\bar{2}$] [111], and [$\bar{1}$10] in grain II, respectively [Fig. 1(a)]. (The shock loading is along the x-axis or the GB normals.) We start with two single crystal supercells, $96 \times 12 \times 20$ grain I (552 960 atoms or ∼600 Å × 100 Å × 100 Å in edge lengths) and $68 \times 17 \times 20$ grain II (554 880 atoms or ∼600 Å × 100 Å × 100 Å in edge lengths), which match in their y-edge lengths. To find the lowest energy GB configuration, we fix grain I and translate grain II along three directions in small steps under three-dimensional boundary conditions, within one atom layer spacing in each direction. For each scan, we perform single-point energy calculation and find that the local energy minimum is located at $\Delta x = 0.7$ Å, $\Delta y = 5.9$ Å, and $\Delta z = 0.6$ Å (shifting grain II with respect to its as-constructed position).

For spallation simulations, two single crystal flyer plates identical to grains I and II are also created for impact on grain I [referred to as the left loading, Fig. 1(b)] and grain II [the right loading, Fig. 1(c)] of the bicrystal, respectively. We perform constant-pressure-temperature simulations on the bicrystal and flyer plates at 150 K and 1 atm for 500 ps before shock simulations. A flyer plate and the bicrystal are assembled along the x-axis (about 1.7×10^6 atoms, or 1800 Å × 100 Å × 100 Å in edge lengths), and the GB is located at $x \approx 600$ Å (the middle

a)Author to whom correspondence should be addressed. Electronic mail: sluo@lanl.gov.
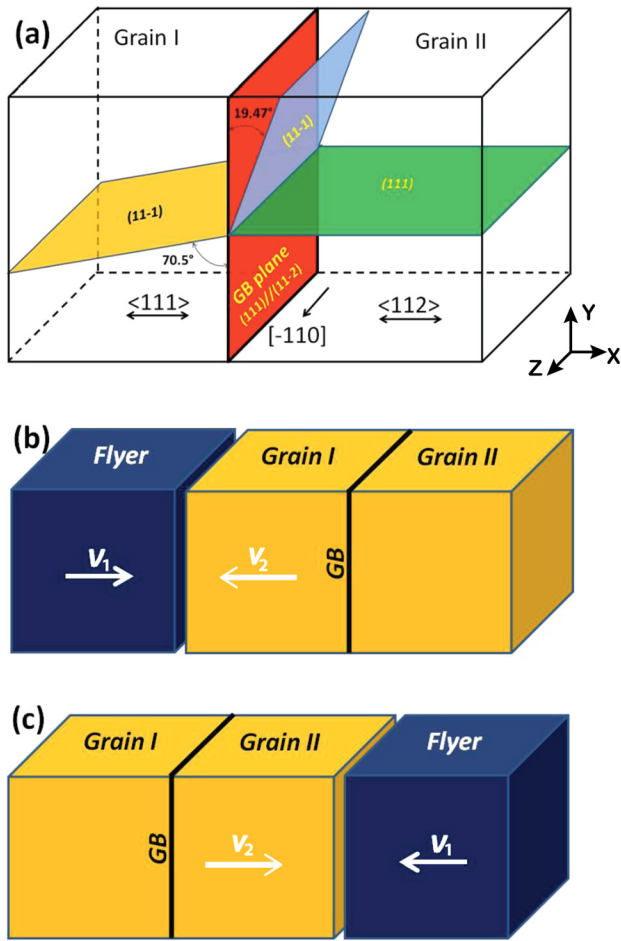
FIG. 1. (Color online) Schematic configuration of the Cu bicrystal (a) and the single crystal flyer plate-bicrystal target impact geometry (b, c). Shock is along the GB normal, and enters the bicrystal either from the left (b) or right (c) to the GB. (b) and (c) are referred to as the left and right loading, respectively. v_1 and v_2 denote the flyer and target velocities, and are $\pm\frac{4}{3}u_\mathrm{p}$ and $\mp\frac{2}{3}u_\mathrm{p}$, respectively. u_p denotes the particle velocity at a supported shock state.

of the bicrystal). We then assign initial velocities of $\pm\frac{2}{3}u_\mathrm{p}$ and $\mp\frac{4}{3}u_\mathrm{p}$ along the x-axis to the bicrystal (target) and flyer plate for impact simulations, respectively. Here u_p denotes the desired "piston velocity." Shock simulations are performed with the microcanonical ensemble, and periodic boundary conditions are only applied along the y- and z-axes. The time step for integrating the equation of motion in all simulations is 1 fs. The local structure is characterized with the centrosymmetry parameter (CSP) (Ref. 21) and coordination number (CN). We use the one-dimensional binning analysis to obtain the wave profiles such as stress (σ_{ij}) profiles. Free surface velocity (u_fs) histories are extracted from the movement of the target free surface (on grain I or II). The von Mises stress σ_vM is defined as ($\sigma_{11} - \frac{1}{2}\sigma_{22} - \frac{1}{2}\sigma_{33}$). The spall strength σ_sp for a given loading is the maximum tensile stress $|\sigma_{11}|$ where spallation occurs. Similar simulation and analysis details can be found elsewhere.[22]

III. RESULTS AND DISCUSSION

Shock simulations are conducted at $u_\mathrm{p} = 0.375$, 0.5, and 0.75 km/s for each loading geometry. We choose these values of u_p in order to observe different degrees of GB plasticity
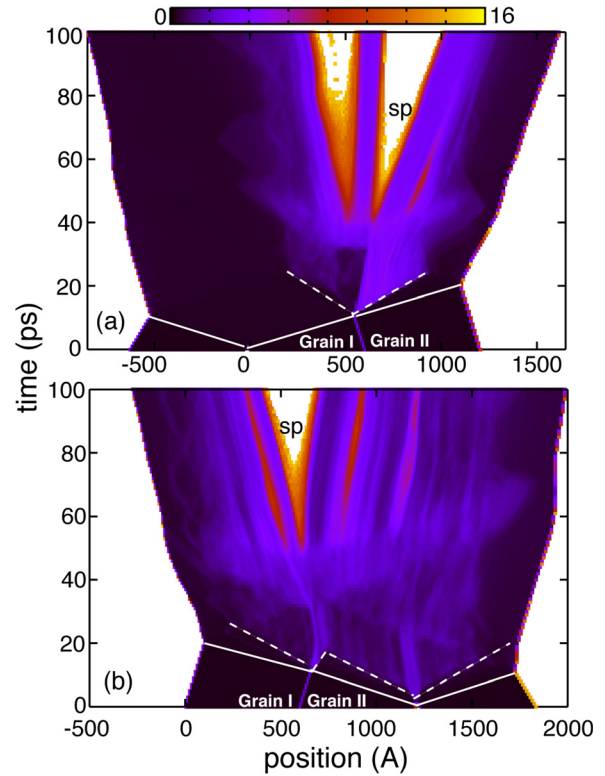

FIG. 2. (Color online) The x-t diagrams in terms of CSP for $u_\mathrm{p} = 0.75$ km/s. (a) is for the left loading and (b) for the right loading, and the impact plane is located at $x = 0$ and $x = 1200$ Å, respectively. The white solid lines indicate the elastic waves, and the dashed lines, plastic waves. sp: spall region.

(negligible to pronounced) and related wave propagation features. The impact yields shock waves propagating into the bicrystal target and the flyer plate, which are then reflected at the respective free surfaces as centered rarefaction fans. These two release fans interact in the bicrystal (near the GB), inducing an evolving tensile region and spallation in the target for sufficiently strong shocks; spallation leads to recompression (even shocks) and free surface velocity pullback. The wave propagation and interactions are illustrated in Figs. 2 and 3 in

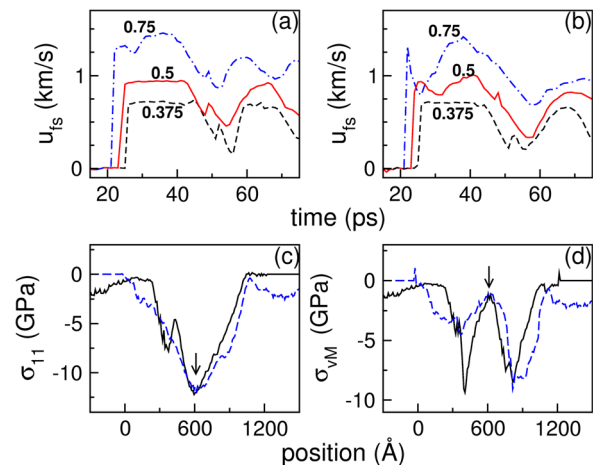FIG. 3. (Color online) $u_\mathrm{fs}(t)$ (a)-(b), and stress profiles during tension (c)-(d). (a)-(b): (a) is for the left loading and (b) for the right loading; numbers denote u_p in km/s. (c)-(d): $\sigma_{11}(x)$ (c) and $\sigma_\mathrm{vM}(x)$ (d) for $u_\mathrm{p} = 0.5$ km/s at $t = 39$ ps and 41 ps, respectively; the solid line denotes the left loading and the dashed line, the right loading.

terms of the position-time $(x-t)$ diagrams, $u_{fs}(t)$ and stress profiles, showing such feature as shock compression, plastic deformation, release fans, and spallation. Waves may undergo reflection and scattering while crossing GB, which may be manifested in different components of, e.g., stress tensor and particle velocity. Our main interest is how the GB asymmetry and the presence or absence of directionality of loading (compression and tension) affect LRLD of the dynamic response of the bicrystal.

For shock compression, the shocks are directional, so LRLD is expected and indeed well manifested in particular for high u_p. The first wave arriving at the GB is elastic. It induces negligible GB plasticity for $u_p = 0.375$ km/s, so $u_{fs}(t)$ is similar both for the left and right loading while minor differences do exist [Figs. 3(a) and 3(b)]. At higher u_p, the elastic shock induces two waves (elastic and plastic) after passing the GB, and the GB plasticity increases with increasing u_p (Fig. 2). For the left loading at 0.5 km/s, the amplitudes of the elastic and plastic waves in grain II are so close that effectively one wave is observed in $u_{fs}(t)$, and the two-wave structure becomes pronounced at 0.75 km/s [Fig. 3(a)]. For the right loading at 0.5 km/s and 0.75 km/s, the elastic-plastic wave feature is more pronounced, but the elastic-plastic transition initiated from the GB is more sluggish (in grain I) than that for the left loading (in grain II) [Figs. 3(a) and 3(b)]. One reason is likely that the slip systems are more difficult to activate in grain I for the right loading, given the geometry of {111} slip planes [Fig. 1(a)]. The preexisting dislocation partials [Fig. 4(a)] in grain II near the GB also facilitate the elastic-plastic transition in grain II for the left loading. As a result, the plastic wave plateau is narrow for the right loading [Fig. 3(b)]. For single crystals, grain I has higher yield strength than grain II, so two waves (elastic and plastic) are induced in grain II before they impinge on the GB at $u_p = 0.75$ km/s for the right loading, while only a single elastic wave is observed in grain I for the left loading

(Fig. 2). Interestingly, the plastic shock initiated from the Grain II interior appears to be impeded by the GB, which is thus both a source and a barrier to dislocations [Fig. 2(b)]. The above observations point to strong LRLD in shock compression response of the (111)//(112)⟨110⟩ bicrystals, in particular when the GB plasticity is involved.

The release fans approach the GB from both sides and induce release and tension. Therefore, the tensile loading lacks directionality. At high u_p (e.g., 0.75 km/s), the microstructure near the GB undergoes modifications during compression, release and tension before spallation, via compressional and tensile plasticity. For low u_p (e.g., 0.375 km/s), compression plasticity is negligible or modest and tensile plasticity is localized around GB with minor modification to the GB region. Regardless of u_p, the GB is the weakest and located in the maximum tension region, so spallation occurs first at GB with the maximum damage [Figs. 2 and 3(c)]. The spall "plane" corresponds to the region with maximum shear stress relaxation [comparing Figs. 3(c) and 3(d)] and thus maximum plasticity. The region of shear stress relaxation [centered at $x \approx$ 600 Å, Fig. 3(d)] is wider for the right loading than the left loading. σ_{sp} is about 11.6, 12.1, and 13 GPa for the left loading (corresponding to $u_p = 0.375$, 0.5, and 0.75 km/s, respectively), slightly higher than those for the right loading (10, 11.5, and 11.9 GPa, respectively), due to the more pronounced GB plasticity for the right loading. The spallation occurs later in the right loading than the left loading and this delay increases with increasing u_p (Figs. 2, 3, and 5), likely because the overall plasticity is more pronounced in the right loading and the effective wave speeds are reduced (Fig. 2). Spallation may occur off the GB, and the off-GB spallation also shows LRLD (Figs. 2 and 5).

The atomic configurations in Fig. 4 illustrate some structure features during compression and tension, using $u_p = 0.5$ km/s as an example. In this bicrystal, there are preexistent partial dislocations in grain II commonly observed for the ⟨112⟩ GB plane
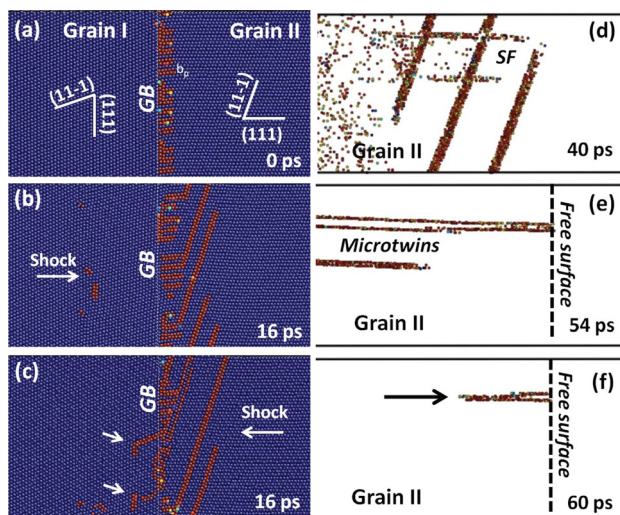

FIG. 4. (Color online) Snapshots of the bicrystal configuration during shock compression (a)-(c) for $u_p = 0.5$ km/s and two loading directions, and microtwinning in grain II (d)-(f) during tension for the left loading. Visualization uses CSP with AtomEye (Ref. 23).
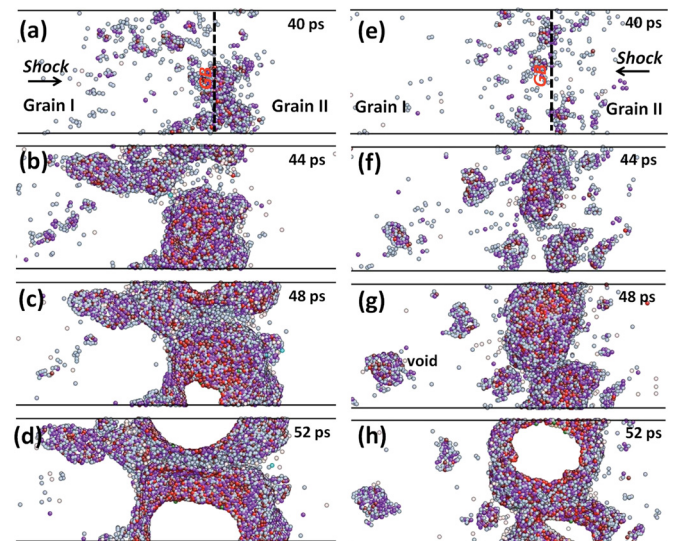

FIG. 5. (Color online) Snapshots of void nucleation and growth for $u_p = 0.5$ km/s and two loading directions. (a)-(d): the left loading, and (e)-(h), the right loading. Only surface atoms enclosing nanovoids (coordination number below 8) are shown.

[Fig. 4(a)]. For shock compression, the GB plasticity triggered by the elastic shock dominates on the grain II side for both loading directions, while the GB plasticity in grain I is more pronounced for the right loading than the left loading [Figs. 4(b) and 4(c); the slanted arrows]. During tension, the overall plasticity in the GB region is more pronounced for the right loading (Fig. 2). Thus, the more "predamage" (prior to spall) in the GB region for right loading leads to slightly smaller σ_{sp} [Figs. 3(c) and 3(d)]. In the tension and spallation stages, we also observe for the left loading that microtwins form and propagate toward grain II free surface and induce a transient surface step [Figs. 4(d)–4(f)]. However, the plasticity in grain II is not pronounced during shock compression so the deformation twinning formed at the tension/spallation stage cannot be locked and is thus unstable and disappears. Microtwinning does not occur in grain I for the right loading. This again points to LRLD due to the structural asymmetry.

Figure 5 compares void nucleation and growth at the same instants for two loading directions. Void nucleation occurs earlier for the left loading than for the right loading, since the effective wave speeds in the former case are faster than those in the latter case [Figs. 5(a) and 5(e)] as discussed above. In both loading cases, the main void nucleation and most damage take place in the GB region due to the GB weakening via, e.g., GB plasticity; the secondary void nucleation is observed mostly in grain I as opposed to grain II, since more slip systems are activated in grain I and their interactions initiate vacancies and disordering for void nucleation.[17,24,25] In contrast, the special orientation of grain II gives rise to preferred shear localization along the $(1\,\bar{1}\,1)$ planes [Figs. 4(b) and 4(c)], and thus less slip systems are activated, so void nucleation is absent in grain II (except the GB-affected region)[14,26] The main damage site is asymmetric with respect to the GB for the left loading via void coalescence (the damage is more severe in grain I); for the right loading, the main damage site is more symmetric in the GB region, with scattered damage sites in grain I. In the later stage of spallation, the damage in grain I for the left loading becomes pronounced as well, while the damage is concentrated at the GB for the right loading (Fig. 2). Compared to the LRLD of shock compression, the LRLD of spallation is more complicated since it depends on the whole process of compression, release and tension, and thus the exact impact geometry. One interesting case to be explored for spallation is that the release wave is initiated only from the bicrystal free surface.

Our simulations show that the loading direction dependence both of plasticity and spall damage may occur for asymmetric GB boundaries; the structural asymmetry at the GB induces differences in plastic deformation and thus spall damage, as well as wave propagation features. The effects of such GBs may be non-negligible or even pronounced in highly structured solids, and should be considered even in developing deformation and damage models for solids with "random" GBs.

IV. CONCLUSION

In summary, our MD simulations of a special asymmetric GB, $(111)//(112)\langle 110\rangle$, demonstrate strong LRLD of its shock response overall, including compression wave features, compression and tensile plasticity, damage characteristics including spall strength, effective wave speeds, and structure changes. However, spallation is still dominated by the GB damage and this feature lacks LRLD as expected. The occurrence of microtwinning during tension/spallation is also loading-direction dependent.

[1]M. A. Meyers, *Dynamic Behavior of Materials* (Wiley, New York, 1994).
[2]G. I. Kanel, Int. J. Fract. **163**, 173 (2010).
[3]M. Meyers and M. Carvalho, Mater. Sci. Eng. **24**, 131 (1976).
[4]W. M. Trott, L. C. Chhabildas, M. R. Baer, and J. N. Castaneda, AIP Conf. Proc. **CP620**, 845 (2002).
[5]E. M. Bringa, A. Caro, M. Victoria, and N. Park, JOM **57**, 67 (2005). Available at http://www.tms.org/pubs/journals/JOM/JOMhome.aspx
[6]V. Dremov, A. Petrovtsev, P. Sapozhnikov, M. Smirnova, D. L. Preston, and M. A. Zocher, Phys. Rev. B **74**, 144110 (2006).
[7]V. V. Dremov, P. A. Sapozhnikov, and E. M. Bringa, AIP Conf. Proc. **CP845**, 387 (2006).
[8]C. Pozzi, T. C. Germann, and R. G. Hoagland, AIP Conf. Proc. **1195**, 765 (2009).
[9]P. Peralta, S. DiGiacomo, S. Hashemian, S. N. Luo, D. Paisley, R. Dickerson, E. Loomis, D. Byler, and K. J. McClellan, Int. J. Damage Mech. **18**, 393413 (2009).
[10]W. J. Zhu, Z. F. Song, X. L. Deng, H. L. He, and X. Y. Cheng, Phys. Rev. B **75**, 024104 (2007).
[11]F. Cao, I. J. Beyerlein, F. L. Addessio, B. H. Sencer, C. P. Trujillo, E. K. Cerreta, and G. T. Gray III, Acta Mater. **58**, 549 (2010).
[12]A. M. Dongare, A. M. Rajendran, B. LaMattina, M. A. Zikry, and D. W. Brenner, J. Appl. Phys. **108**, 113518 (2010).
[13]L. Wayne, K. Krishnan, S. DiGiacomo, N. Kovvali, P. Peralta, S. N. Luo, S. Greenfield, D. Byler, D. Paisley, K. J. McClellan, A. Koskelo, and R. Dickerson, Scr. Mater. **63**, 1065 (2010).
[14]S. N. Luo, T. C. Germann, D. L. Tonks, and Q. An, J. Appl. Phys. **108**, 093526 (2010).
[15]H. H. Pham, B. Arman, S. N. Luo, and T. Cagin, J. Appl. Phys. **109**, 086107 (2011).
[16]B. L. Holian, Shock Waves **5**, 149 (1995).
[17]S. G. Srinivasan, M. I. Baskes, and G. J. Wagner, J. Appl. Phys. **101**, 043504 (2007).
[18]Y. Mishin, M. J. Mehl, D. A. Papaconstantopoulos, A. F. Voter, and J. D. Kress, Phys. Rev. B **63**, 224106 (2001).
[19]S. Plimpton, J. Comp. Phys. **117**, 1 (1995). See http://lammps.sandia.gov.
[20]Y. C. Wang, Z. X. Sun, and D. H. Ping, J. Mater. Sci. Technol. **26**, 1047 (2010).
[21]C. L. Kelchner, S. J. Plimpton, and J. C. Hamilton, Phys. Rev. B **58**, 11085 (1998).
[22]S. N. Luo, Q. An, T. C. Germann, and L. B. Han, J. Appl. Phys. **106**, 013502 (2009).
[23]J. Li, Modell. Modell. Simul. Mater. Sci. Eng. **11**, 173 (2003).
[24]S. N. Luo, T. C. Germann, and D. L. Tonks, J. Appl. Phys. **106**, 123518 (2009).
[25]Y. Ashkenazy and R. S. Averback, Appl. Phys. Lett. **86**, 051907 (2005).
[26]P. Peralta and C. Laird, Acta Mater. **45**, 3029 (1997).